Aromaticity

DOI: 10.1002/anie.201104166

Aromatic Metal-Centered Monocyclic Boron Rings: $Co©B_8^-$ and $Ru©B_9^-$**

Constantin Romanescu, Timur R. Galeev, Wei-Li Li, Alexander I. Boldyrev, and Lai-Sheng Wang**

Bulk boron, which is characterized by 3D cage-like structural features, is a refractory material.[1,2] However, 3D cage structures were suggested to be unstable for small boron clusters, and planar or quasi-planar structures have been proposed instead.[3–5] Experimental studies combined with high-level calculations have shown that small boron cluster ions are planar up to at least B_{20}^-,[6–10] whereas B_n^+ ions have been found to be planar up to $n = 16$.[11] The chemical bonding in the planar boron clusters has been found to be quite remarkable;[6–9] in addition to the strong and localized bonding in the circumferences, there are two types of delocalized bonding—the in-plane σ and the out-of-plane π bonding, each of which follows the $(4N + 2)$ Hückel rule for aromaticity. In particular, systems with six σ and six π electrons ($N = 1$) are doubly aromatic, and give rise to highly symmetric planar clusters, such as B_8^{2-} and B_9^-, which each contain a central B atom and a B_7 and B_8 monocyclic ring, respectively.[6] In the D_{7h} B_8^{2-} and D_{8h} B_9^- molecular wheels, each B atom in the circumference contributes two electrons to the B–B peripheral covalent bonds and one electron to the delocalized bonds, whereas the central B atom contributes all its valence electrons to the delocalized bonds. These novel bonding situations suggest that other atoms with appropriate numbers of valence electrons and sizes may be able to replace the central boron atom to produce $M©B_n$-type clusters.[12]

Hexagonal, heptagonal, and octagonal $C©B_n$-type clusters have been proposed from theoretical calculations as examples of hexa-, hepta-, and octacoordinate planar carbons.[13–15] However, photoelectron spectroscopy (PES) studies showed that carbon occupies the peripheral position in such clusters rather than the center,[16,17] because C is more electronegative than B and thus prefers to participate in localized two-center-two-electron (2c-2e) σ bonding, which is possible only at the circumference of the wheel structure. Transition-metal atoms are better suited for the central position in the $M©B_n$ clusters, as these metals favor participation in delocalized bonding at the center over localized bonding at the periphery. For an $M©B_n$ cluster, the electronic requirement for the central atom is $x = 12-n$ or $x = 12-n-k$ for an $M©B_n^{k-}$ anion, where x is the valence of the transition-metal atom M, in order to satisfy the peripheral B–B σ bonding and the σ and π Hückel aromaticity for $N = 1$. Indeed, all 3d transition-metal atoms have been tested computationally for the $M©B_n$-type hypercoordinate complexes.[18–21] Two complexes, namely $Co©B_8^-$ and $Fe©B_9^-$, in which the Co and Fe atoms are trivalent and divalent, respectively, were found to be closed-shell global minima, in agreement with our electronic design principle.

We have focused our experimental efforts on transition-metal-doped boron clusters that involve Group 8 (Fe, Ru, Os) and 9 (Co, Rh, Ir) elements. The experiments were carried out using a PES apparatus equipped with a laser vaporization supersonic cluster source and a magnetic-bottle PES analyzer (see the Experimental Section). Spectra were obtained for a wide range of MB_n^- clusters. The spectra of CoB_8^- and RuB_9^- (Figure 1) were different, in that, they both displayed relatively high electron binding energies and simple spectral patterns (see Figure S1 in the Supporting Information for a comparison of the spectra of RuB_n^- for $n = 3$–10).[22] The first adiabatic detachment energies (ADEs) and the vertical detachment energies (VDEs) of all the spectral features for the two doped boron clusters are given in Table 1 and are

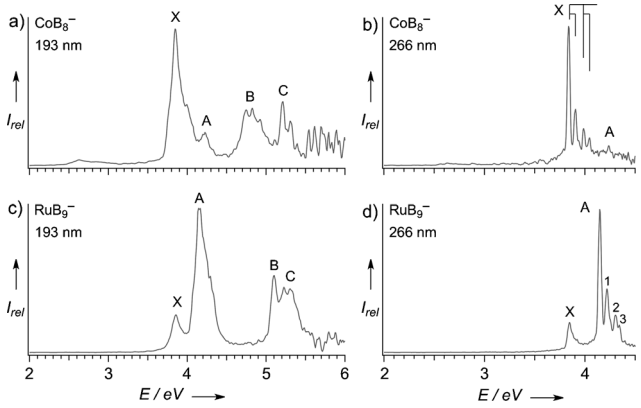

Figure 1. Photoelectron spectra of CoB_8^- at a) 193 nm (6.424 eV) and b) 266 nm (4.661 eV). Photoelectron spectra of RuB_9^- at c) 193 nm and d) 266 nm. The vertical lines in (b) and the numbers in (d) indicate vibrational structures.

[*] Dr. C. Romanescu, W. L. Li, Prof. Dr. L. S. Wang
Department of Chemistry, Brown University
Providence, RI 02912 (USA)
E-mail: lai-sheng_wang@brown.edu
Homepage: http://www.chem.usu.edu/~boldyrev/
T. R. Galeev, Prof. Dr. A. I. Boldyrev
Department of Chemistry and Biochemistry, Utah State University
Logan, UT 84322 (USA)
E-mail: a.i.boldyrev@usu.edu

[**] This work was supported by the National Science Foundation (DMR-0904034 to L.S.W. and CHE-1057746 to A.I.B.). Computer times from the Centers for High Performance Computing at the University of Utah and Utah State University are gratefully acknowledged. T.R.G. wishes to thank USU for the Vice President for Research Graduate Fellowship.

Supporting information for this article is available on the WWW under http://dx.doi.org/10.1002/anie.201104166.

compared with theoretical calculations. Four detachment features (X, A–C) were observed for CoB_8^- (Figure 1a).[23] At 266 nm (Figure 1b), the X band was vibrationally resolved: two vibrational modes were observed, one with a frequency of (1200 ± 50) cm^{-1} and another with a frequency of (520 ± 50) cm^{-1}. The A band was weak at 193 nm (Figure 1a) and became even weaker at 266 nm (Figure 1b). Four well-resolved bands (X, A–C) were also observed in the spectrum of RuB_9^- (Figure 1c). At 266 nm (Figure 1d), the X band was observed to be fairly sharp without any resolved vibrational structures, thus suggesting that a very low frequency mode was involved and that there was little geometry change between the anion and the neutral ground state. The A band of RuB_9^- was vibrationally resolved with three vibrational modes (Figure 1d): (550 ± 50), (1240 ± 50), and (1560 ± 50) cm^{-1}. The simple spectral patterns and the resolved vibrational structures for such complicated systems suggest that CoB_8^- and RuB_9^- should have high symmetries.

To confirm the symmetries of CoB_8^- and RuB_9^-, we optimized their structures (see Experimental Section) and found that the D_{8h} $Co©B_8^-$ ($^1A_{1g}$, $\ldots 3a_{1g}^{\ 2}2e_{1u}^{\ 4}$) and D_{9h} $Ru©B_9^-$ ($^1A_1'$, $\ldots 2e_1'^4 3a_1'^2$) are indeed minima on the potential energy surfaces (Figure 2). Our result for $Co©B_8^-$ is consistent with previous calculations.[20] We computed the VDEs for these clusters at several levels of theory (Table 1) and found excellent agreement with the experimental data. Optimization of the neutral clusters led to a lower symmetry D_{2h} $Co©B_8$ and a C_{9v} $Ru©B_9$ (Figure 2). The actual structural distortions are relatively minor. The Ru atom is only approximately 0.1 Å out of plane in the neutral C_{9v} RuB_9. The highest occupied molecular orbital (HOMO) of the D_{8h} $Co©B_8^-$ is degenerate ($2e_{1u}$). Detachment of an electron from the $2e_{1u}$ HOMO results in Jahn–Teller distortions that reduce the symmetry of $Co©B_8$ to D_{2h}. We calculated the vibrational frequencies of the D_{2h} $Co©B_8$ and found four totally symmetric modes: 442 (ν_1), 549 (ν_2), 754 (ν_3), and 1160 (ν_4) cm^{-1}. The frequencies of two of these modes (ν_2 and ν_4), which are responsible for the D_{8h} to D_{2h} distortion, are in excellent agreement with the observed vibrational frequencies of (520 ± 50) and (1200 ± 50) cm^{-1} in the X band of the photoelectron spectrum (Figure 1b). The calculated ADE of CoB_8^- is also in excellent agreement with the experimental value (Table 1).

The HOMO of the D_{9h} $Ru©B_9^-$ is $3a_1'$, which is primarily of Ru $4d_{z^2}$ character (Figure S2). The out-of-plane distortion is consistent with the nature of this HOMO. This structural distortion suggests that the vibrational mode, which is active upon removing an electron from the HOMO, should involve the Ru atom moving up and down. This mode has a calculated frequency of 36 cm^{-1}, which is in agreement with the unresolved low frequency vibration of the X band (Figure 1d). The HOMO-1 ($2e_1'$) of $Ru©B_9^-$ is degenerate and Jahn–Teller distortions are expected for detachment from this orbital, consistent with the observed vibrational features in the A band (Figure 1d). The calculated

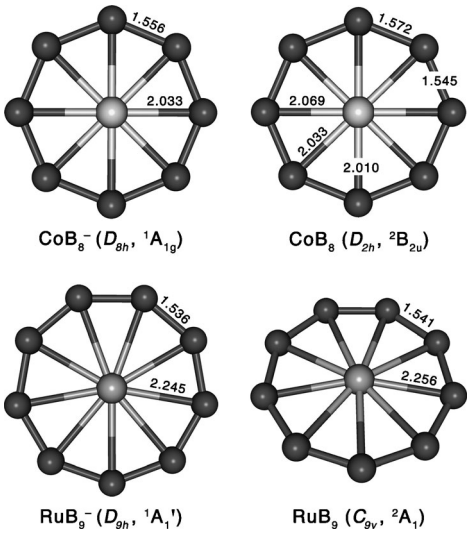

Figure 2. Optimized structures for $Co©B_8^-$, $Co©B_8$, $Ru©B_9^-$, and $Ru©B_9$. The structures presented are at the PBE1PBE/6-311+G* level for $Co©B_8^-$ and $Co©B_8$ and PBE1PBE/Ru/Stuttgart/B/aug-cc-pvTZ level for $Ru©B_9^-$ and $Ru©B_9$ (see Experimental Section). Symmetries and spectroscopic states are given in the parentheses. Bond lengths are given in Å.

Table 1: Comparison between experimental and theoretical results. Observed vertical electron detachment energies (VDEs) for CoB_8^- and RuB_9^- compared with theoretical values calculated from the D_{8h} $Co©B_8^-$ ($^1A_{1g}$) and D_{9h} $Ru©B_9^-$ ($^1A_1'$).

Observed features	VDE (exp)[a]	Final state and electronic configuration	VDE (theo)		
			PBE1PBE[b]	B3LYP[c]	ROCCSD(T)[d]
		$Co©B_8^-$ (D_{8h}, $^1A_{1g}$)			
X[e]	3.84 (1)	$^2E_{1u} \ldots 1b_{2g}^{\ 2}\,1e_{1g}^{\ 4}\,2e_{2g}^{\ 4}\,1a_{2u}^{\ 2}\,3a_{1g}^{\ 2}\,2e_{1u}^{\ 3}$	3.81	3.72	3.88
A	4.23 (2)	$^2A_{1g} \ldots 1b_{2g}^{\ 2}\,1e_{1g}^{\ 4}\,2e_{2g}^{\ 4}\,1a_{2u}^{\ 2}\,3a_{1g}^{\ 1}\,2e_{1u}^{\ 4}$	3.90	3.97	4.20
B	4.82 (3)	$^2E_{2g} \ldots 1b_{2g}^{\ 2}\,1e_{1g}^{\ 4}\,2e_{2g}^{\ 3}\,1a_{2u}^{\ 2}\,3a_{1g}^{\ 2}\,2e_{1u}^{\ 4}$	4.60	4.58	4.82
C	5.21 (4)	$^2E_{1g} \ldots 1b_{2g}^{\ 2}\,1e_{1g}^{\ 3}\,2e_{2g}^{\ 4}\,1a_{2u}^{\ 2}\,3a_{1g}^{\ 2}\,2e_{1u}^{\ 4}$	5.12	5.17	5.58
–	–	$^2A_{2u} \ldots 1b_{2g}^{\ 2}\,1e_{1g}^{\ 4}\,2e_{2g}^{\ 4}\,1a_{2u}^{\ 1}\,3a_{1g}^{\ 2}\,2e_{1u}^{\ 4}$	5.27	5.15	
		$Ru©B_9^-$ (D_{9h}, $^1A_1'$)			
X[f]	3.85 (1)	$^2A_1' \ldots 2a_1'^2\,1e_1''^4\,2e_2'^4\,1a_2''^2\,2e_1'^4\,3a_1'^1$	3.68	3.70	3.80
A[g]	4.15 (1)	$^2E_1' \ldots 2a_1'^2\,1e_1''^4\,2e_2'^4\,1a_2''^2\,2e_1'^3\,3a_1'^2$	4.17	4.05	4.28
B	5.11 (3)	$^2E_2' \ldots 2a_1'^2\,1e_1''^4\,2e_2'^3\,1a_2''^2\,2e_1'^4\,3a_1'^2$	5.22	5.12	5.30
C	5.29 (3)	$^2A_2'' \ldots 2a_1'^2\,1e_1''^4\,2e_2'^4\,1a_2''^1\,2e_1'^4\,3a_1'^2$	5.30	5.16	5.45

[a] Numbers in parentheses represent the uncertainty in the last digit. [b] VDEs for $Co©B_8^-$ were calculated at ROPBE1PBE/6-311+G(2df)//PBE1PBE/6-311+G*; VDEs for $Ru©B_9^-$ were calculated at ROPBE1PBE/Ru/Stuttgart/B/aug-cc-pvTZ. [c] VDEs for $Co©B_8^-$ were calculated at ROB3LYP/6-311+G(2df)//B3LYP/6-311+G*; VDEs for $Ru©B_9^-$ were calculated at ROB3LYP/Ru/Stuttgart/B/aug-cc-pvTZ. [d] VDEs for $Co©B_8^-$ were calculated at ROCCSD(T)/6-311+G(2df)//PBE1PBE/6-311+G*. VDEs for $Ru©B_9^-$ were calculated at ROCCSD(T)/Ru/Stuttgart/B/aug-cc-pvTZ//PBE1PBE/Ru/Stuttgart/B/aug-cc-pvTZ. [e] Measured adiabatic detachment energy (ADE) is the same as the VDE. Calculated ADE at ROCCSD(T)/6-311+G(2df)//PBE1PBE/6-311+G* with ZPE correction is 3.78 eV. [f] Measured ADE = (3.83 ± 0.02) eV. Calculated ADE at ROCCSD(T)/Ru/Stuttgart/B/aug-cc-pvTZ//PBE1PBE/Ru/Stuttgart/B/aug-cc-pvTZ with ZPE correction = 3.75 eV. [g] Observed vibrational frequencies: (550 ± 50), (1240 ± 50), and (1560 ± 50) cm^{-1}.

ADE of $Ru©B_9^-$ is also in good agreement with the experimental value (Table 1). Overall, the theoretical results and the experimental observations are in excellent agreement, thus confirming unequivocally that the D_{8h} $Co©B_8^-$ and D_{9h} $Ru©B_9^-$ structures are highly stable and should be the global minima on their respective potential energy surfaces.

The valence MOs for the D_{8h} $Co©B_8^-$ and D_{9h} $Ru©B_9^-$ are shown in Figure S2. The MOs responsible for the B–B bonding in the circumference, the delocalized π bonding (HOMO-2 ($1a_{2u}$) and HOMO-4 ($1e_{1g}$) for $Co©B_8^-$; HOMO-2 ($1a_2''$) and HOMO-4 ($1e_1''$) for $Ru©B_9^-$), and the delocalized σ bonding (HOMO ($2e_{1u}$) and HOMO-6 ($2a_{1g}$) for $Co©B_8^-$; HOMO-1 ($2e_1'$) and HOMO-5 ($2a_1'$) for $Ru©B_9^-$) can be readily recognized. Each complex contains six delocalized π and six delocalized σ electrons, thus resulting in double aromaticity and high electronic stability. Each complex also has three primarily d-based orbitals (d_{z^2}, d_{xy}, and $d_{x^2-y^2}$), which can also be readily recognized. The adaptive natural density partitioning (AdNDP) analyses[24] show the bonding situations in the two complexes more clearly (Figure 3). These results show the lone pairs of electrons in the d orbitals, the B–B peripheral bonds, and the double aromaticity in both clusters. The occupation numbers for the localized and delocalized MOs are all close to 2. However, the two d-based MOs (d_{xy} and $d_{x^2-y^2}$) have occupation numbers significantly less than 2 (1.81 | e | in CoB_8^- and 1.65 | e | in RuB_9^-), thus suggesting that these MOs are involved in covalent interactions between the monocyclic ligands and the central metal atoms with the contribution of the 4d element (Ru) being higher than that of the 3d element (Co). Co is formally trivalent in $Co©B_8^-$ and Ru is formally divalent in $Ru©B_9^-$, consistent with our electronic design principle.

According to this design principle, the smaller the B_n ring, the higher the required valence of the central atom M. For example, for a B_6 ring, a hexavalent atom is required for $M©B_6$ or a pentavalent atom for an $M©B_6^-$ ion. The C-centered CB_6^{2-} and CB_7^-, which were studied computationally,[13] are consistent with our design principle, even though they are not the global minima.[16,17] Geometrical effects, that is, the size of the central atom has to be appropriate for optimal stability of the $M©B_n$ clusters, dictate that the B_6 or even the B_7 ring is too small to host a transition-metal atom in the center. Thus, the B_8 and B_9 rings are optimal for hosting a central transition-metal atom. The B_{10} ring is most likely too large to host a divalent (for $M©B_{10}$) or monovalent atom (for $M©B_{10}^-$). For example, the global minimum of AuB_{10}^- has been shown to be an Au atom that interacts with a B_{10} cluster on its periphery, whilst the D_{10h} $Au©B_{10}^-$, albeit a local minimum, is much higher in energy.[25]

The first transition-metal atom centered in a planar monocyclic ring appears to be $Fe©Sn_5^+$ and $Fe©Bi_5^+$, although these structures are not the global minima on their respective potential energy surfaces.[26] The $Co©B_8^-$ and $Ru©B_9^-$ clusters reported here are unprecedented in chemistry with coordination numbers of 8 and 9 in perfect planar environments. The $M©B_n^-$ systems are unique because of the ability of boron to form multicenter bonds and the ensuring multiple aromaticity. Because of the central position of the transition-metal atom in $M©B_n^-$, appropriate ligands may be conceived for coordination above and below the molecular plane, thus rendering chemical protection and allowing syntheses of this new class of novel boron-based metal complexes with unexpected chemical properties.

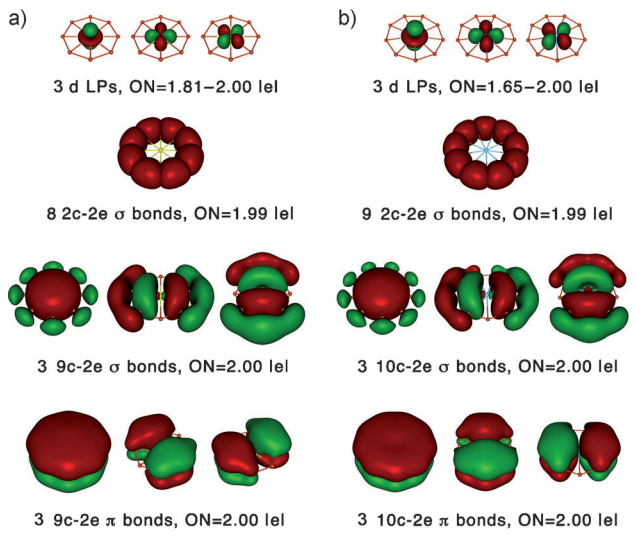

Figure 3. a) AdNDP analysis for $Co©B_8^-$. b) AdNDP analysis for $Ru©B_9^-$. The 2c-2e σ-bonds are superimposed on the circumference B–B framework. Note the double aromaticity derived from the three delocalized σ and π bonds in each cluster.

Experimental Section

Photoelectron spectroscopy: Mixed boron (enriched in ^{11}B) and transition metal (M) targets were ablated by a pulsed laser. Clusters formed from the laser-induced plasma were entrained into a helium carrier gas and underwent a supersonic expansion. Anions in the cold cluster beam were analyzed using a time-of-flight mass spectrometer. Clusters of interest were selected by a mass gate and decelerated before being intercepted by a laser beam. Two detachment photon energies were used: 193 nm (6.424 eV) from an ArF excimer laser and 266 nm (4.661 eV) from a Nd:YAG laser. Photoelectrons were analyzed by a magnetic-bottle-type analyzer and calibrated by the known spectrum of Bi^-. The electron binding energy spectra presented in Figure 1 were obtained by subtracting the kinetic energy spectra from the respective photon energies. The electron kinetic energy resolution of the apparatus was $\Delta E_k/E_k \approx 2.5\,\%$, that is, about 25 meV for 1 eV electrons.[27]

Theoretical calculations: Geometry optimizations and frequency analyses for $Co©B_8^-$ and $Co©B_8$ were performed using the PBE1PBE and B3LYP hybrid density functionals with the 6–311 + G* basis set. VDE and ADE calculations were performed at three levels of theory: ROCCSD(T)/6–311 + G(2df) and ROPBE1PBE/6–311 + G(2df) (both at PBE1PBE/6–311 + G* geometries) and ROB3LYP/6–311 + G(2df)//B3LYP/6–311 + G*. ROPBE1PBE/Ru/Stuttgart/B/aug-cc-pvTZ and ROB3LYP/Ru/Stuttgart/B/aug-cc-pvTZ were used for similar calculations on $Ru©B_9^-$ and $Ru©B_9$. VDE and ADE values were also calculated at ROCCSD(T)/Ru/Stuttgart/B/aug-cc-pvTZ (at PBE1PBE/Ru/Stuttgart/B/aug-cc-pvTZ geometries). Chemical bonding analyses (PBE1PBE/LANL2DZ) of both clusters were performed using the AdNDP method.[24] All calculations were carried out using Gaussian 03 and Gaussian 09.[28] Molekel 5.4.0.8 was used for MO visualization.[29]

Received: June 16, 2011
Published online: August 31, 2011

Keywords: aromaticity · boron · cluster compounds · coordination modes · transition metals

[1] H. Hubert, B. Devouard, L. A. J. Garvie, M. O'Keeffe, P. R. Buseck, W. T. Petuskey, P. F. McMillan, *Nature* **1998**, *391*, 376.
[2] M. Fujimori, T. Nakata, T. Nakayama, E. Nishibori, K. Kimura, M. Takata, M. Sakata, *Phys. Rev. Lett.* **1999**, *82*, 4452.
[3] R. Kawai, J. H. Weare, *J. Chem. Phys.* **1991**, *95*, 1151.
[4] A. Ricca, C. W. Bauschlicher, *Chem. Phys.* **1996**, *208*, 233.
[5] I. Boustani, *Phys. Rev. B* **1997**, *55*, 16426.
[6] H. J. Zhai, A. N. Alexandrova, K. A. Birch, A. I. Boldyrev, L. S. Wang, *Angew. Chem.* **2003**, *115*, 6186; *Angew. Chem. Int. Ed.* **2003**, *42*, 6004.
[7] H. J. Zhai, B. Kiran, Li, J., L. S. Wang, *Nat. Mater.* **2003**, *2*, 827.
[8] A. P. Sergeeva, D. Y. Zubarev, H. J. Zhai, A. I. Boldyrev, L. S. Wang, *J. Am. Chem. Soc.* **2008**, *130*, 7244.
[9] W. Huang, A. P. Sergeeva, H. J. Zhai, B. B. Averkiev, L. S. Wang, A. I. Boldyrev, *Nat. Chem.* **2010**, *2*, 202.
[10] B. Kiran, S. Bulusu, H. J. Zhai, S. Yoo, X. C. Zeng, L. S. Wang, *Proc. Natl. Acad. Sci. USA* **2005**, *102*, 961.
[11] E. Oger, N. R. M. Crawford, R. Kelting, P. Weis, M. M. Kappes, R. Ahlrichs, *Angew. Chem.* **2007**, *119*, 8656; *Angew. Chem. Int. Ed.* **2007**, *46*, 8503.
[12] The @ sign has already been used to indicate endohedral doping in 3D cage clusters, such as in $He@C_{60}$ or $Cu@Au_{16}$. We propose the © sign to designate the central position of the doped atom in monocyclic structures in $M©B_n$-type planar clusters.
[13] K. Exner, P. von R. Schleyer, *Science* **2000**, *290*, 1937.
[14] Z. X. Wang, P. von R. Schleyer, *Science* **2001**, *292*, 2465.
[15] R. M. Minyaev, T. N. Gribanova, A. G. Starikov, V. I. Minkin, *Mendeleev Commun.* **2001**, *11*, 213.
[16] L. M. Wang, W. Huang, B. B. Averkiev, A. I. Boldyrev, L. S. Wang, *Angew. Chem.* **2007**, *119*, 4634; *Angew. Chem. Int. Ed.* **2007**, *46*, 4550.
[17] B. B. Averkiev, D. Y. Zubarev, L. M. Wang, W. Huang, L. S. Wang, A. I. Boldyrev, *J. Am. Chem. Soc.* **2008**, *130*, 9248 – 9250.
[18] Q. Luo, *Sci. China Ser. B* **2008**, *51*, 607.
[19] Q. Y. Wu, Y. P. Tang, X. H. Zhang, *Sci. China Ser. B* **2009**, *52*, 288.
[20] K. Ito, Z. Pu, Q. S. Li, P. von R. Schleyer, *Inorg. Chem.* **2008**, *47*, 10906.
[21] Z. Pu, K. Ito, P. von R. Schleyer, Q. S. Li, *Inorg. Chem.* **2009**, *48*, 10679.
[22] Although D_{9h} FeB_9^- was suggested to be a closed-shell global minimum (Ref. [20]), its photoelectron spectrum displays broad features, thus indicating the existence of possible low-lying isomers.
[23] The weak signal near 2.6 eV was likely due to the presence of a triplet excited state of CoB_8^- in the cluster beam, which would be metastable and long-lived. The signals above 5.5 eV were too noisy to allow identification of definitive spectral transitions.
[24] D. Y. Zubarev, A. I. Boldyrev, *Phys. Chem. Chem. Phys.* **2008**, *10*, 5207.
[25] H. J. Zhai, C. Q. Miao, S. D. Li, L. S. Wang, *J. Phys. Chem. A* **2010**, *114*, 12155.
[26] M. Lein, J. Frunzke, G. Frenking, *Angew. Chem.* **2003**, *115*, 1341; *Angew. Chem. Int. Ed.* **2003**, *42*, 1303.
[27] L. S. Wang, H. S. Cheng, J. Fan, *J. Chem. Phys.* **1995**, *102*, 9480.
[28] M. J. Frisch, et al., GAUSSIAN 03, Rev. C.02, Gaussian, Inc., Wallingford, CT, **2004** and GAUSSIAN 09, Rev. B.01, Gaussian, Inc., Wallingford, CT, **2009**.
[29] U. Varetto, Molekel 5.4.0.8, Swiss National Supercomputing Centre, Manno, Switzerland, 2009.

